Lake Ice Cover Deflection Induced by Moving Vehicles: Comparing Theoretical Results with Satellite Observations

Hossein Babaei[*1], Joost van der Sanden[+], Naomi Short[+] and Paul Barrette[*]

*) Ocean, Coastal and River Engineering, National Research Council of Canada, Ottawa
+) Canada Centre for Remote Sensing, Natural Resources Canada, Ottawa

Paper prepared for presentation at the *NEW RESEARCH AND DEVELOPMENTS IN ROAD SAFETY* Session of the 2016 Conference of the Transportation Association of Canada Toronto, ON

Abstract

Ice roads are essential to the livelihood of several communities and the operations of several industries in Canada's North. Safe yet maximized exploitation of such roads is paramount to all stakeholders. Through a state-of-the-art remote sensing technology, ice road deformations because of transportation activities over a lake in the Northwest Territories, Canada have been recently measured. In the present paper, the dynamic response of the ice road is theoretically modelled and model results were compared with the remotely-sensed deformations. Comparisons are for two different cases of a slow truck whose motion does not create any significant waves in the ice cover, and a fast truck whose motion creates wave patterns in the ice cover. Remotely-sensed and theoretical deformations, for both cases, compare well. It is then concluded that both the theoretical model and the satellite-derived product could assist in safety and operations improvements of ice roads on lakes. Some preliminary conclusions that may help guide ice road operations are given.

Introduction

Ice roads are an important part of the way of life in the North. They are used to move both people and goods into regions which otherwise would not be accessible in the winter. Ice roads have implications to both an individual's way of life as well as northern industry. For example, ice roads are used to bring in large quantities of food and material to the diamond mines located in the Northwest Territories (NWT) of Canada which otherwise would have to be flown in at much greater expense. The NWT's government, industry and local communities work together to try to ensure safe roads. However, as activities in the North are expected to intensify, and in the context of a warming climate, a decrease in the average number of 'freezing degree-days' means that ice road builders will have to do more with less, i.e. increased activity with a reduced operational lifespan, without compromising the safety of the operations. Various means of counteracting this phenomenon may be envisaged. One is through an improved understanding of ice bearing capacity which may support the optimization of traffic variables including maximum speeds and vehicle interspacing.

In February 2015, two Synthetic Aperture Radar (SAR) satellites comprised in the TanDEM-X mission from the German Aerospace Centre (DLR) and EADS Astrium GmbH (Krieger et al., 2013) imaged the Tibbitt-to-Contwoyto Winter Road (TCWR) in the NWT. Ice cover displacement products obtained

[1] babaeih@nrc.ca

through analysis of the resulting data were found to display effects of moving vehicles (van der Sanden and Short, 2016). In this paper, we will capitalize on a unique and unprecedented opportunity to compare the information contained in these products with theoretical predictions of the dynamic response of a floating ice plate. A theoretical analysis of this type of loading is followed by comparison and discussion of theoretical ice deflections and displacement patterns measured by TanDEM-X. Some preliminary conclusions that may help guide the operation of the TCWR and others like it will be drawn.

The Tibbit-to-Conwoyto Winter Road (TCWR)

The Tibbitt to Contwoyto winter road begins at Tibbitt Lake at the end of Highway 4 about 60 kilometres east of Yellowknife, Northwest Territories, Canada. From there, it winds its way north linking four diamond mines – Ekati, Diavik, Snap Lake, and finally Tahera at the north end of Contwoyto Lake, Nunavut Territory. The total length of the TCWR is 600 kilometres, about 85% of which is over lake ice. This is a region served by no other highways, and for 10 months of the year it is only accessible by air. The road is open during 8-10 weeks every winter, usually starting by the end of January. The road opens when the ice thickness is about 1.07 m and comprises two to three lanes with a width of about 50 meters each.

TCWR is an important supply line for the mines. Each winter, the TCWR sees between 5,000 and 10,000 truckloads, with gross weight up to 40 metric tons (and sometimes more). Diesel fuel is one of the main items that is trucked up to the mines (www.jvtcwinterroad.ca). Other supplies include cement, tires, ammonium nitrate (for the fabrication of explosives) and various construction materials. There are strict guidelines for the usage of the road (TC WRJV "Winter road regulations and rules of the road," 2015). Notably, the maximum speed for driving on lakes is 25 km/h for loaded trucks and could be up to 60 km/h for unloaded trucks. Also, drivers must maintain 500 m spacing between trucks at all times.

This study focusses on a section of the TCWR on Gordon Lake (Figure 1). Gordon Lake is one of the larger lakes used by the TCWR. It has a maximum length of 45 km, a maximum width of 6.5 km and a maximum depth exceeding 85 m (Moore, 1981).

Remotely-sensed Ice Road Displacements

The capacity of SAR satellites to measure the vertical displacement of ice cover by moving vehicles was explained in van der Sanden and Short (2016). Briefly, this capacity hinges on advanced satellite SAR technology that enables the acquisition of two matching images within seconds for subsequent analysis by means of differential interferometric radar data (DInSAR) processing techniques. For the TanDEM-X data applied in this study, the time lapse between the first acquisition at time T1 and the second at time T2 was 10-seconds. Figure 2 depicts the relationship between, simulated, DInSAR measurements and deflections that may be measured with the help of conventional in situ devices. Definitive numbers regarding the accuracy of DInSAR measurements are hard to give because it depends on the fidelity of an applied external DEM as well as a mix of SAR system and acquisition variables including the operating wavelength, the orbital data quality, the coherence level and the atmosphere's stability. The coherence ranges from 0 to 1 and signifies the quality of the DInSAR measurements. Low and high coherence values denote doubtful and reliable measurements, respectively. Lower coherence values result from temporal change, i.e. from T1 to T2, in the radar reflection characteristics of the object observed. Extending from the results shown in van der Sanden and Short (2016), the accuracy of the satellite

measurements presented in the current paper is estimated to be better than about 1 mm 90% of the time provided the associated coherence is ≥ 0.6. DInSAR measurements corresponding to moving vehicles, rather than surrounding unchanging ice cover, are likely to have lower coherence levels and therefore reduced accuracies (down to about 5 mm). The TanDEM-X displacement products utilized for the purpose of this study were geocoded to the UTM WGS84 coordinate system with a pixel spacing of 4 m by 4 m.

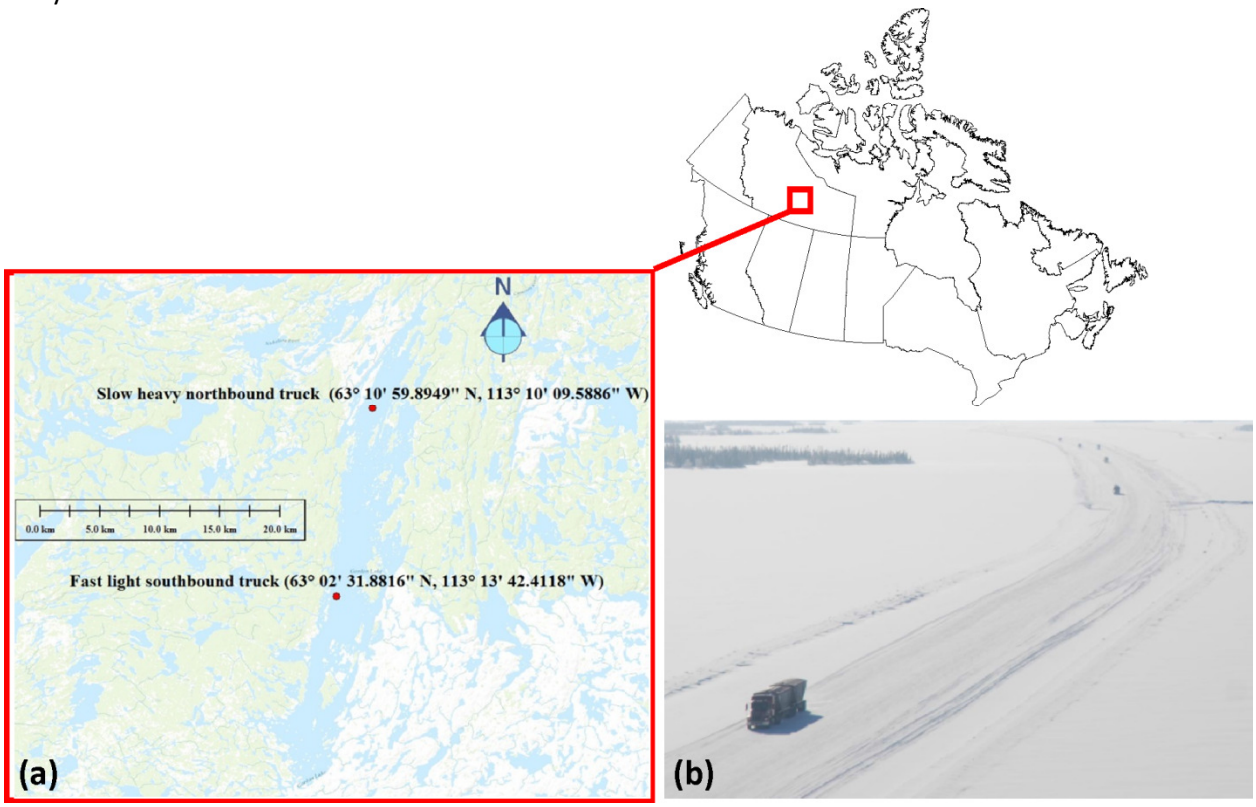

Figure 1. (a) Gordon Lake in Northwest Territories, Canada – the locations of the vertical displacement patterns shown in Figures 3 and 7 are marked (b) Vehicles travelling along the TCWR on Gordon Lake (February 2013).

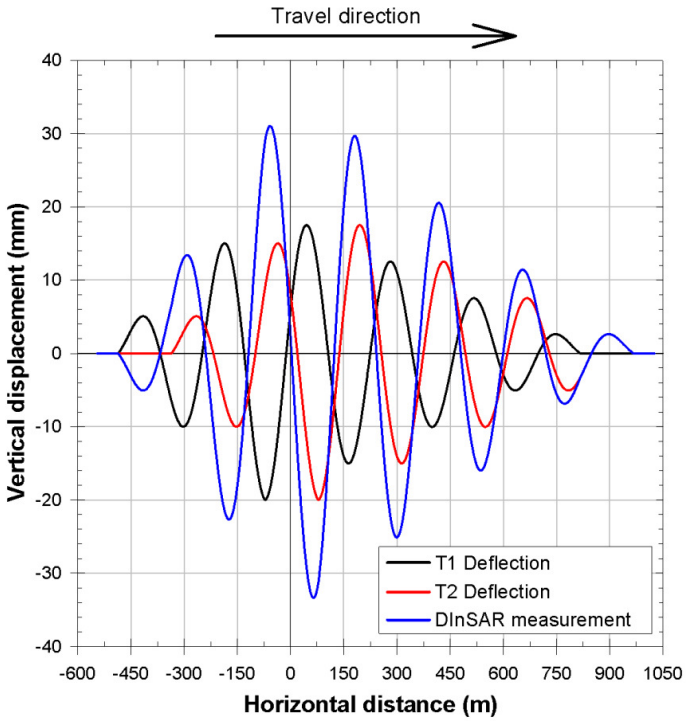

Figure 2. Simulated plots illustrating the use of differential SAR interferometry (DInSAR) to measure ice cover vertical displacements along the travel path of a moving vehicle. The DInSAR measurements equal the superposition of the T2 deflection and the inverse of the T1 deflection. The T1 to T2 time interval is assumed to be 10 seconds. In Figure 2, the moving vehicle responsible for the ice deflection is assumed to be located at a distance of 0 m at T1 and to travel at a speed of 15 m s^{-1} (van der Sanden and Short, 2016).

Theoretical Modelling of the Steady Response of a Thin Floating Ice Plate Loaded by a Moving Load

This classical mechanics problem has been the topic of several past research works. Here, we briefly review the literature on the coupled solid-fluid mechanics modelling of the problem. For a more detailed literature review, we suggest the book of Squire et al. (1996). Kheysin (1963) was a pioneer to model the underneath fluid as an "actual" fluid rather than an elastic foundation. He studied point and line loads for shallow waters and examined what speeds lead to theoretical deflection singularities. Although original and valuable, his work involved some calculation mistakes. Nevel (1970) corrected Kheysin (1963) work for the point load case and lifted the shallow water condition limitations. He also extended the point load assumption to uniform circular loads. Nevel (1970), however, only calculated ice plate's deflections and stresses under the load center. Davys et al. (1985) studied far-field wave patterns and deflection amplitudes in ice plates loaded by a point load and compared some of their results with deflection measurements of an ice runway at McMurdo Sound, Antarctica. They showed that steady deflection wave will occur only if the speed of the load exceeds the so-called 'critical speed', an important concept in ice road operations. At that stage, and in theory, the deflections will grow with time limitlessly. They showed that the wave patterns in the ice plate strongly depend on the speed of the moving load and that when the speed is very large, no wave exists over a zone behind the load. They named this zone the shadow zone. Milinazzo et al. (1995) lifted the far field limitation of Davys et al. (1985) and also extended the point load limitation of Davys et al. (1985) work by modelling uniformly

distributed loads over rectangular regions. They calculated ice plate deflections everywhere including regions close and far from the load. They also confirmed the existence of a shadow zone behind very fast loads as predicted by Davys et al. (1985) and compared some of their results with the experimental work of Takizawa (1988).

Problem Definition and Formulation

Consider a load moving with a constant velocity on an ice plate floating on a fluid. We now look at the theory for the ice response under these conditions. Doing so, we make some simplifying assumptions:

The plate is assumed to be thin with small deflections relative to its thickness and that:

1- The middle plane of the plate does not deform. The middle plane is then neutral which means in-plane external loads can be neglected.
2- Planes normal to the neutral plane remain normal to it, which means the resulting shear deflections of the plate can be neglected.
3- The normal stresses along the plate thickness are negligible relative to in-plane stresses which means the three-dimensionality of the problem can be neglected, which allows simplification into a two-dimensional problem.

To learn more about the validity conditions of the above assumptions, see Timoshenko and Woinowsky-Krieger (1959).

In addition to the above, we are assuming that the plate is homogeneous and isotropic, behaving linearly elastically and has a uniform thickness.

Moreover, the substrate fluid is assumed to be Newtonian, incompressible, invicid and its flow is assumed to be irrotational. The Euler-Bernoulli's equation could then be used for the fluid dynamics of the problem. The fluid is further assumed to have a uniform density and depth.

Based on the above assumptions, the governing equations of the problem in steady state case in a frame of reference moving with the load are (Nevel 1970; Davys et al. 1985; Milinazzo et. al 1995):

$$D\left(\eta_{xxxx} + \eta_{yyyy}\right) - p + \rho_{ice} h u^2 \eta_{xx} = -P(x,y) \quad (1a)$$

$$\phi_{xx} + \phi_{yy} + \phi_{zz} = 0 \quad (1b)$$

$$g\eta + \frac{p}{\rho} + u\phi_x|_{z=0} = 0 \quad (1c)$$

$$\phi_z|_{z=-H} = 0 \quad (1d)$$

$$\phi_z|_{z=0} = u\eta_x \quad (1e)$$

where η, p, and ϕ are respectively the vertical displacement of the middle plane of the plate (positive when upward), pressure at the water-plate interface, and the fluid velocity potential. ρ_{ice}, ρ, and D are the density of ice, the density of water, and the flexural rigidity of the plate $\left(D = \frac{Eh^3}{12(1-\nu^2)}\right)$ where E is the effective Young's modulus, h is the plate thickness, and ν is the plate's Poisson's ratio. g, u, and P are the gravitational acceleration, the speed of the moving source and its weight. H is the depth of the fluid and subscripts denote partial differentiation. Note that the above equations are in the Cartesian coordinate system moving with the load along the +x direction and the +z direction is upward.

Equations (1a) through (1c) respectively govern the equilibrium of the plate, conservation of mass of the fluid, and the coupling between the solid and fluid mechanics of the problem. Equations (1d) and (1e) satisfy the conditions of a zero normal-to-lakebed fluid velocity (z component), and the equality of the velocity of the fluid and the velocity of the plate at the interface (z component). Note that equation (1c) is based on the linearized form of the Euler-Bernoulli's equation and equation (1e) is valid only when the vertical displacement of the plate is small.

The solution of the governing equations could be obtained by the Fourier transform technique:

$$\eta = -\frac{1}{2\pi}\int_{-\infty}^{\infty}\int_{-\infty}^{\infty}\frac{\hat{P}(l,m)}{B(l,m)}e^{-i(lx+my)}dldm \tag{2a}$$

$$B(l,m) = Dk^4 + \rho g - \rho_{ice}hu^2l^2 - \frac{\rho u^2 l^2}{k}coth(kH) \tag{2b}$$

The details of the solution procedure to obtain equations (2) could be found in Nevel (1970) and Davys et al. (1985).

$\hat{P}(l,m)$ is the Fourier transform of the load $P(x,y)$ and $k^2 = l^2 + m^2$. i is the unit imaginary number. If a steady wave pattern with respect to the moving load exists:

$$ul = \omega \tag{3}$$

where ω is the frequency. Equation (3) satisfies the condition that the component of the load velocity normal to any wave crest must be equal to the speed of the wave crest. In this condition the equation $B(l,m) = 0$ and k are known as the dispersion relation and the wavenumber, respectively.

The phase speed of the present dispersion relation, $\frac{\omega}{k}$, has a global minimum that we denote by c_{min}. No steady disturbance could then travel more slowly than this speed. This means that when the speed of the load is less than c_{min}, no steady waves will exist and disturbances will move away from the load. This c_{min} is usually named the critical speed. Experimentations show that deflections of ice roads are pronounced when the speed of the load approaches c_{min} (Wilson, 1955; 1985), (Sunberg-Falkenmark, 1963), (Beltaos, 1981) and (Takizawa, 1978). The critical speed is found by intersecting the phase speed curve $\frac{\omega(k)}{k}$ ($\omega(k)$ is the frequency as a function of the wavenumber) with the group speed curve ($\frac{d\omega}{dk}$); phase speed and group speed could be found from the dispersion relation. On a day-to-day ice road operation, guidelines use the critical speed concept to limit vehicle speed. In other words, truck drivers are told not to exceed what is thought to be the critical speed, so as to reduce the amount of ice road deflection and the likelihood of ice failure. Such ice failure has been observed to occur as a consequence.

Comparison of Theoretical Ice Deflections and Wave Characteristics with Satellite-derived Data

The theoretical response of TCWR at Gordon Lake is studied in this section. The results of the study are then compared with the satellite-derived data. Two different cases are considered: (1) the response to the motion of a slow heavy northbound truck, and (2) the response to the motion of a fast light southbound truck. Figure 1a showed the location of the trucks on the lake.

Table 1 lists relevant properties of the ice road, loading conditions, and the depth of the lake for each case. Note that for both cases, theoretical results based on two different ice thicknesses are presented. In addition, for the southbound case, theoretical results based on two different effective Young's moduli values are presented. The reasons for these two different thicknesses and effective Young's moduli will be given later in the paper.

Table 1. Ice road properties, loading conditions, and the depth of the lake for each case.

		Slow heavy northbound case	**Fast light southbound case**
	$g, m/s^2$	**9.81**	
Truck	$u, m/s\ (km/h)$	**7(25.2)**	**16(57.6)**
	M,(Mass), kg	**40000**	**20000**
Ice road	$\rho_{ice}, kg/m^3$	**917**	
	h, m	**1.07 & 1.375**	**1.07 & 1.375**
	ν	$1/3$	
	E, GPa	**5**	**5 & 7.6**
Lake	$\rho, kg/m^3$	**1000**	
	H, m	**17.5**	**22.5**

For each case, truck speed, given in Table 1, was estimated based on the distance between the minimum and maximum values of the satellite-derived data in the neighbourhood of the truck. The estimated speed values were corroborated by consulting with TCWR's safety guidelines and authorities (Anonymous, 2015). Typical truck weight for loaded (heavy) and unloaded (light) values obtained from TCWR Joint Venture website (http://www.jvtcwinterroad.ca/) and authorities. A local person experienced in fishing in the area provided the lake depth data which was in part obtained by a depth-measuring device. Although Gordon Lake consists of several islands and rocky shoals, the lake depth is believed to be consistent over a large region in the locations of interest.

Table 2 lists the critical speed values, calculated by a numerical root finding scheme, for the two different locations based on the ice road and lake-related data given in Table 1. For investigated cases, the critical speed does not vary significantly.

Table 2. The critical speed, c_{min} , for the northbound, in curved brackets, and the southbound, shown with bolded font, cases for different effective Young moduli and ice road thicknesses. Note that other parameters affecting the critical speed are given in Table 1.

		h	
		1.07 m	1.375 m
E	5 GPa	**13.99 m/s** (12.75 m/s)	**14.36 m/s** (12.91 m/s)
	7.6 GPa	**14.24 m/s**	**14.51 m/s**

The trucks of interest on the TCWR are typically Super B Train trucks (see Fig. 4a) whose trailers are supported by seven axles with four wheels on each axle (two on each side of the truck). Other types of vehicles use this winter road, but for the purpose of this exercise, we assume the patterns observed from the satellite images are from these trucks. We model the moving truck as a concentrated point

load, .i.e., $\widehat{P}(l,m) = -\frac{Mg}{2\pi}$, where M is the truck mass. We, however, consider the reality that the truck weight is distributed over all its wheels. We provide more details later.

The case of the slow heavy northbound truck

Figure 3 shows the 10-seconds vertical displacement of the ice road surface for the northbound case derived from the satellite data acquired on February 10th, 2015. The new location of the truck is associated with negative values, visualized by shades of blue, because ice road surface has moved down in this region compared to 10 s earlier. The previous location of the truck is associated with positive values, visualized by shades of red, because the truck surface has moved up within a 10-second interval. No wave pattern is seen for this case which is consistent with the prediction of the theoretical model; the truck speed (7 m/s) is well below the critical speed for this northbound case which is over 12 m/s, as given in Table 2.

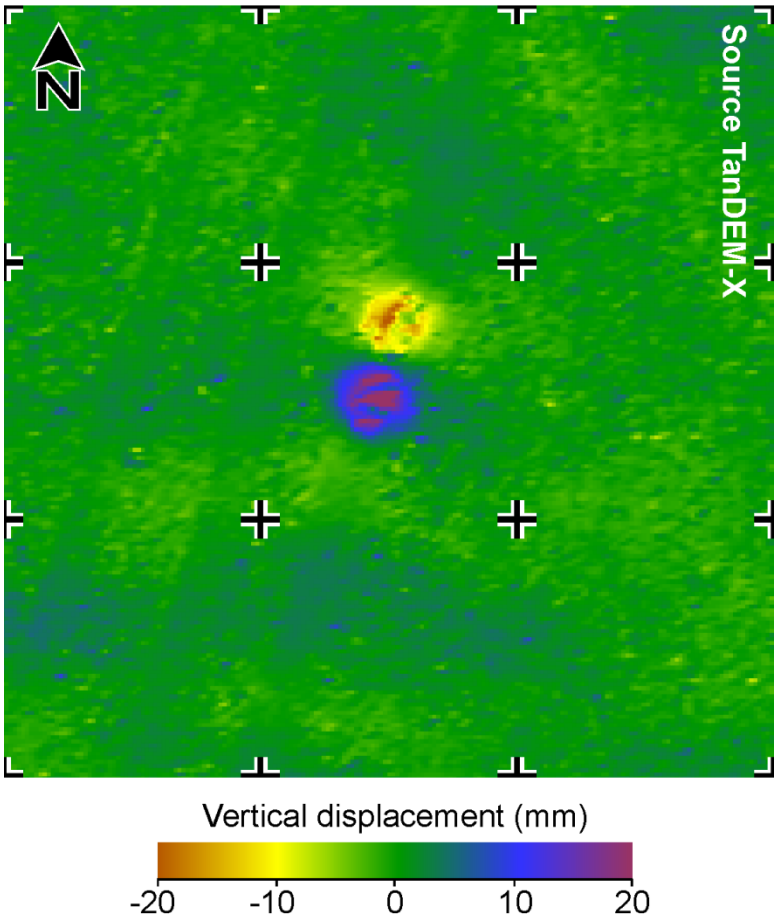

Figure 3. Satellite-derived 10-seconds vertical displacement of the ice road surface induced by a heavy slow northbound vehicle. The spacing of the overlaid cross grid is 250 m by 250 m.

For the theoretical modelling of the problem, the moving truck is modelled as fourteen moving point loads shown by red circles in Figure 4b. Each of the two back and front trailer axles bear 1/8th of the load while each of the three middle trailer axles bear 1/6th of the load. The truck weight is distributed evenly

along the y axis. Spacing between axles and the truck width are typical values for the Super B train trucks, (www.richardstransport.com/equipment and www.transportation.alberta.ca/Content/docType281/production/B-train.pdf)

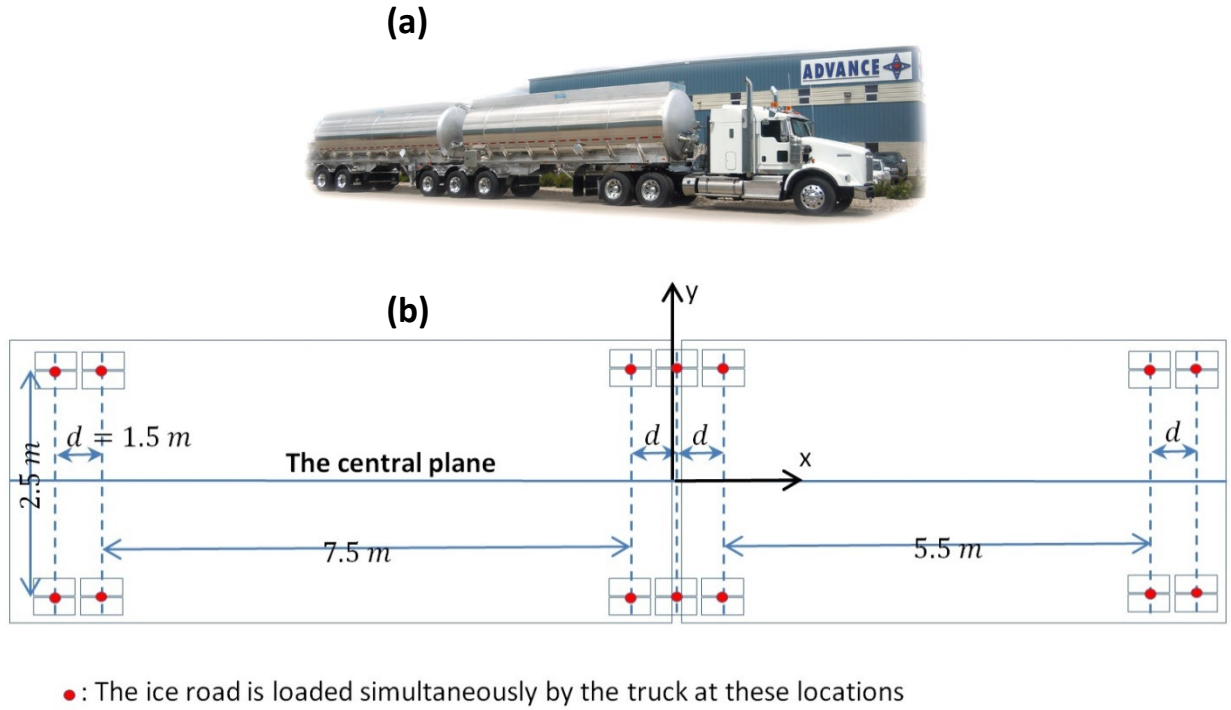

Figure 4. (a) Super B Train (http://www.advanceengineeredproducts.com with permission from AEPL) (b) Schematic of the aerial view of the truck trailers and axles (not to scale).

The deflection of the ice road is given by Equation 2a. The integral is calculated by an iterative numerical method based on a quadrature technique implemented by MATLAB technical computing environment. The integration's absolute and relative tolerances are both 1e-8. The deflection of the central plane, shown in Figure 4b, caused by each of the fourteen moving point loads are superimposed to calculate the total deflection. Figure 5 shows the deflection of the central plane at t = 0 s and at t = 10 s, and also the 10-seconds vertical displacement for two different ice thicknesses. Figure 5 also depicts the 10-seconds vertical displacement based on the satellite data. The satellite-related curve in that figure is extracted on a line connecting the extremums of Figure 3. This line is approximately along the ice road.

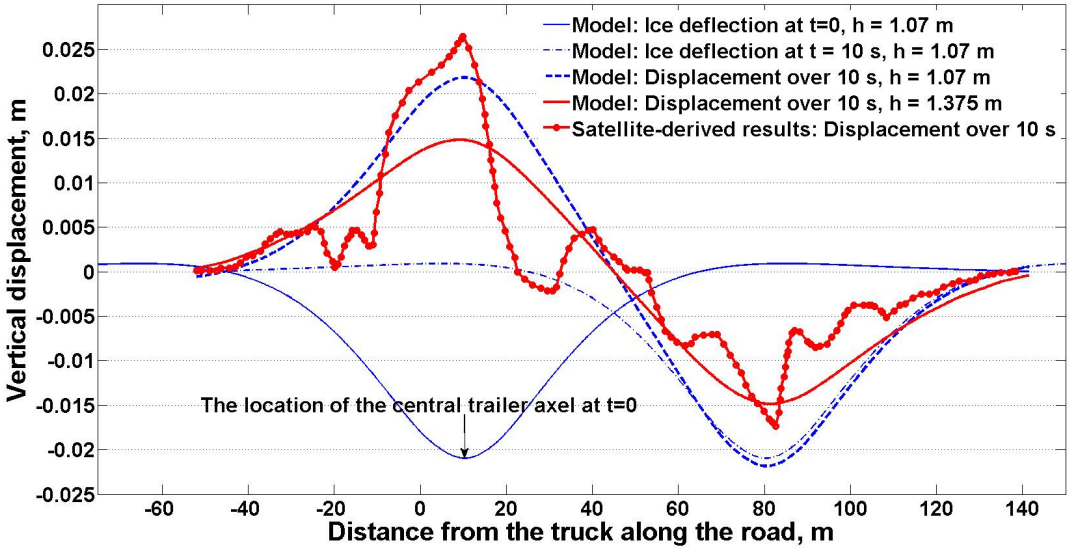

Figure 5. The theoretical and satellite-derived displacements of the ice road surface for the northbound case. Two different ice road thicknesses are considered. Satellite data source TanDEM-X, © DLR 2015.

The thickness of the TWCR at Gordon Lake is a function of time. The two considered thickness values of 1.07 m and 1.375 m are early and late season values in the operational period of the road. The date of the satellite data is Feb. 10th, 2015 so the ice road thickness is probably closer to the larger modelled thickness. Note that the variation in the thickness of the lake ice cover as a function of location is probably smaller early in season than it is later in the season. This difference in the variability results from activities such as snow removal and forced flooding that aim to increase ice thickness or repair damages to the road surface. The present theoretical model does not account for this variability in the ice cover's thickness.

The horizontal extent of the downward deflection of the road based on the model and the satellite data are consistent despite the loss of coherence in satellite image in regions alternatingly occupied by a vehicle and ice cover.

Normal in-plane stresses at the bottom of the ice road can be calculated, numerically based on the calculated deflections, by the following equations:

$$\sigma_{xx} = \frac{E}{1-\nu^2}\frac{h}{2}\left(\eta_{xx} + \nu\eta_{yy}\right)$$
$$\sigma_{yy} = \frac{E}{1-\nu^2}\frac{h}{2}\left(\eta_{yy} + \nu\eta_{xx}\right) \quad (4)$$

Figure 6a shows the stresses for the two thicknesses. Note that sudden fluctuations in the tail portions of the stress curves in Figure 6a are because of integration noise and need to be ignored. The y component of the normal stress is larger than the x component of the normal stress. This means that when the truck is very heavy, cracks will be along the road rather than across of it. This is supported by the shape of the cracks in Figure 6b that shows an incident happening recently to a loaded moving truck in an ice road near Déline, NWT. The calculated stresses for the northbound case are below the ultimate

tensile strength of ice. The recommended allowed tensile strength in ice roads is between $5 \times 10^5\ Pa$ to $7 \times 10^5 Pa$ (Hayley and Proskin, 2008; Masterson, 2009) although the ultimate tensile strength of ice samples in laboratories could be as high as $17 \times 10^5 Pa$ (Timco and O'Brien, 1994). The reason is that this allows for a safety factor of about 3.0 against first crack failure (Masterson, 2009).

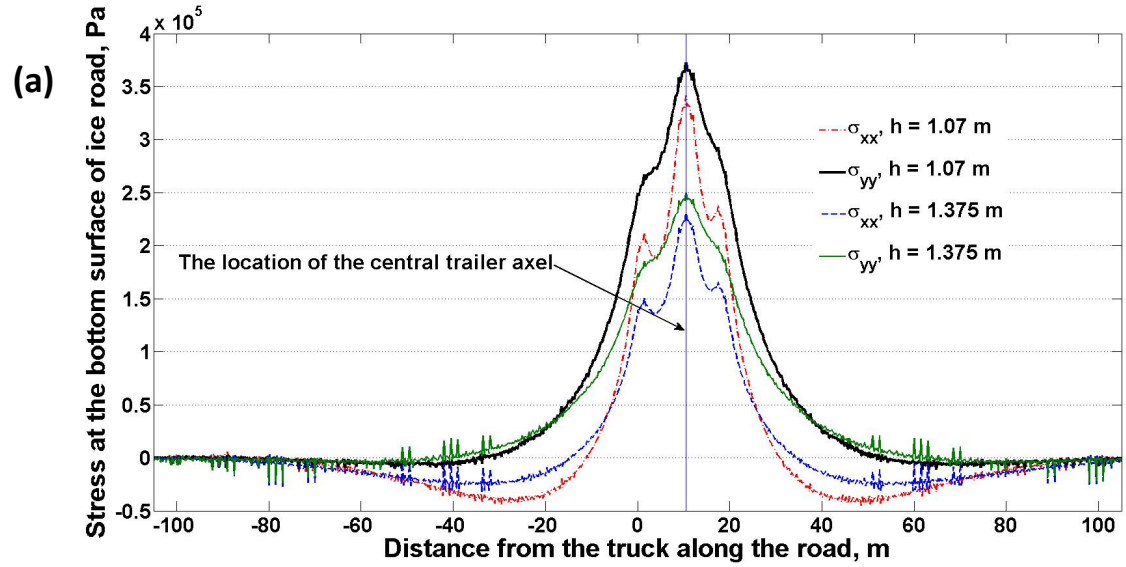

Figure 6. (a) The theoretical normal stresses at the bottom of the ice road along the road for two different ice road thicknesses for the northbound case. Fluctuations in tail regions are integration noise and can be overlooked. (b) A recent, March 2016, incident in an ice road near Deline, NWT happening for a loaded moving truck. The circumstances that led to this incident are unknown to the authors as of this writing. The crack shapes suggest that an along-the-road crack has happened before an across-the-road crack. Picture is courtesy of NWT Environment and Natural Resources.

The case of the fast light southbound truck

Figure 7 shows the 10-seconds vertical displacement of the ice road surface for the southbound case derived from satellite data acquired on February 9th, 2015. Wave patterns are obvious in the figure. The theoretical critical speed for this case is 14.51 m/s or lower (depending on ice thickness and effective Young's modulus given in Table 1) while the approximate truck speed is 16 m/s. Since the truck speed is larger than the critical speed, the theoretical model predicts steady wave pattern in the ice cover. This prediction is consistent with the satellite-derived observations shown in Figure 7.

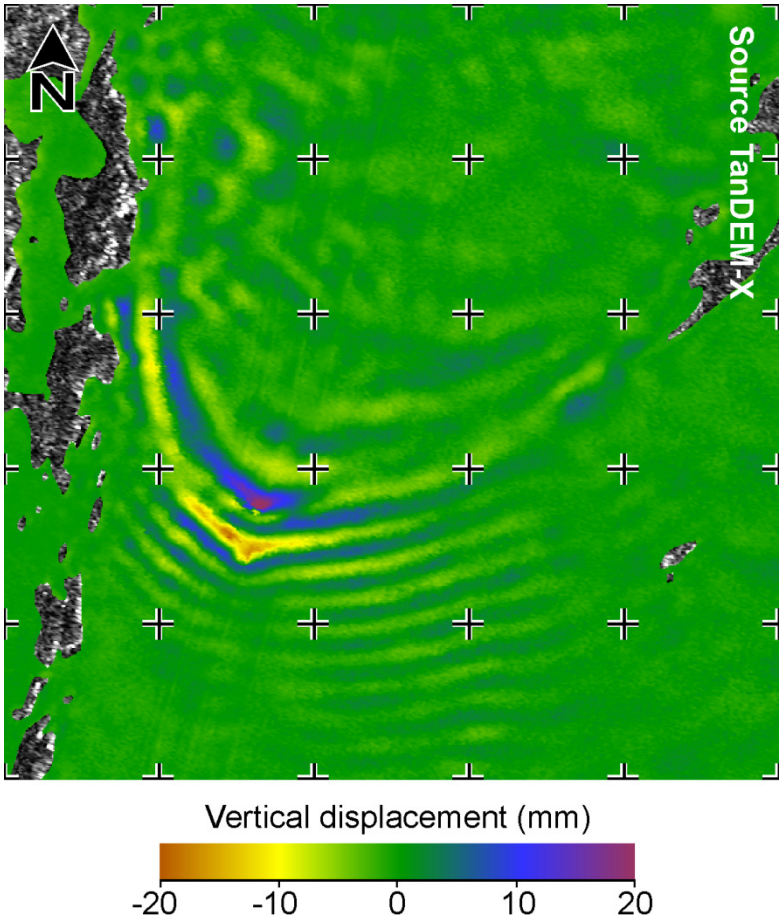

Figure 7. Satellite-derived 10-seconds vertical displacement of the ice road surface for the southbound case. Wave patterns are seen in the figure. The existence of waves is also predicted theoretically since the truck speed is larger than the theoretical critical speed for this case. The spacing of the overlaid cross grid is 500 m by 500 m.

To compare the theoretically predicted wave patterns and ice deflections with the satellite-derived results, Equations (2a) must be solved. When the speed of the moving load is larger than the critical speed, the integral in Equation (2a) is singular on a closed curved line named the wavenumber curve. Because of this singularity, exact solution of the integral is generally impossible and its numerical treatment is generally much more complex than the case when this singularity is absent. This complexity could be completely avoided if the governing equations of the problem, Equations (1), are directly solved numerically by finite-element, finite-different or similar techniques. We do not seek the direct numerical solution of the governing equations in the present paper. We avoid the complexity of

this integral by seeking asymptotic methods. The limitation of asymptotic methods, however, is its probable invalidity close to the location of the moving load. For details of asymptotic methods see the book of Lighthill (1978). The asymptotic solution for Equation (2a) is (Davys et al. 1985):

$$\eta \approx -\hat{P}(l_0, m_0)\left[\left(\frac{\partial B}{\partial n}\right)_0\right]^{-1}\left(\frac{2\pi}{|\kappa_0| r}\right)^{0.5} e^{-i(l_0 x + m_0 y + \Theta)} \tag{5}$$

where κ, Θ, and r are respectively the curvature of the wavenumber curve in the lm plane, a phase shift factor, and the distance from the moving load, $r^2 = x^2 + y^2$. The phase shift factor is $\pi/4$ if $\kappa \times n_l > 0$ and $3\pi/4$ otherwise. $\boldsymbol{n}$ is the outward unit normal to the wavenumber curve and n_l is the component of $\boldsymbol{n}$ along the l direction. $\frac{\partial B}{\partial n}$ is the directional derivative of the wavenumber curve with respect to $\boldsymbol{n}$, however, for the calculation of η the sign of this derivative must be changed if $n_l < 0$. Note that the deflection given by the above equation is evaluated at any given point on the wavenumber curve, e.g. point T_0 shown in Figure 8, and a given phase, $K = \boldsymbol{k_0} \cdot \boldsymbol{r}$. Equation (5) is invalid if T_0 is an inflection point of the wavenumber curve and/or if there is any other location on the curve at which $\boldsymbol{n} = \boldsymbol{n_{T_0}}$. For these two invalid conditions, Equation (5) must be revised; Davys et al. (1985) provides the revised versions. In the present paper, we only evaluate the deflections on the x axis along which Equation (5) is valid. The polar coordinates of constant-phase locations in the xy plane are $\left(\frac{K}{k_0 cos(\chi)}, \theta\right)$.

Note that Figure 8 is the upper half of the wavenumber curve which is always symmetric with respect to the l axis. The bisection method was used to find many, out of infinity, roots of the dispersion relation.

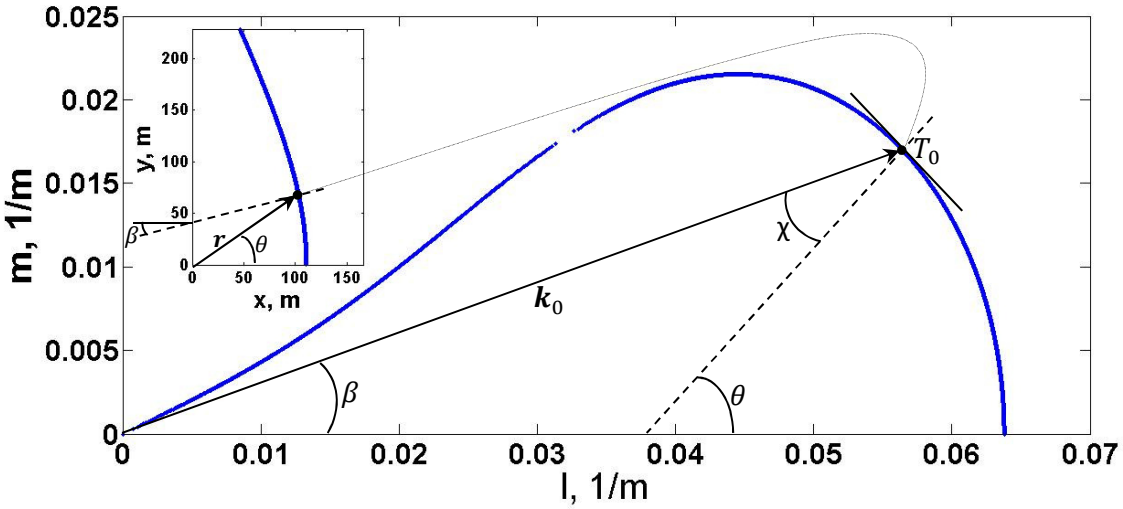

Figure 8. The upper half of the wavenumber curve for $E = 5\ GPa$ and $h = 1.07\ m$ and other properties and conditions given in Table 1. The smaller subplot is the wave pattern corresponding to the phase value of $K = \frac{9\pi}{4} rad.$

We have plotted and overlaid theoretical wave patterns on the satellite-derived data in Figure 9. To avoid the complexity of superimposing wave patterns cased by each of the truck wheels, the wave pattern shown in Figure 9 corresponds to a single concentrated moving load when $E = 5\ GPa$ and

$h = 1.07\ m$ while other properties and conditions are given in Table 1. Note that the theoretical wave patterns show a zone behind the truck over which no wave exists. This is the shadow zone alluded to earlier in this paper, which is also shown in Figure 10 over a larger region on the xy plane. The existence of the shadow zone is theoretically expected when the speed of the moving load exceeds $\sqrt{gH}$ which is the celerity of free surface waves in shallow waters. This is the case for the present southbound case since the truck speed, 16 m/s, is larger than $\sqrt{gH}$ ≈14.86 m/s. A careful investigation of the satellite-derived data shown in Figure 7 and/or Figure 9 reveals that the road behind the truck is less disturbed than the road in front of the truck; there is a well defined wave pattern in front of the truck while except one to two distinct wave-like disturbances, the road behind of the truck does not show a high level of disturbance. This supports the existence of the shadow zone.

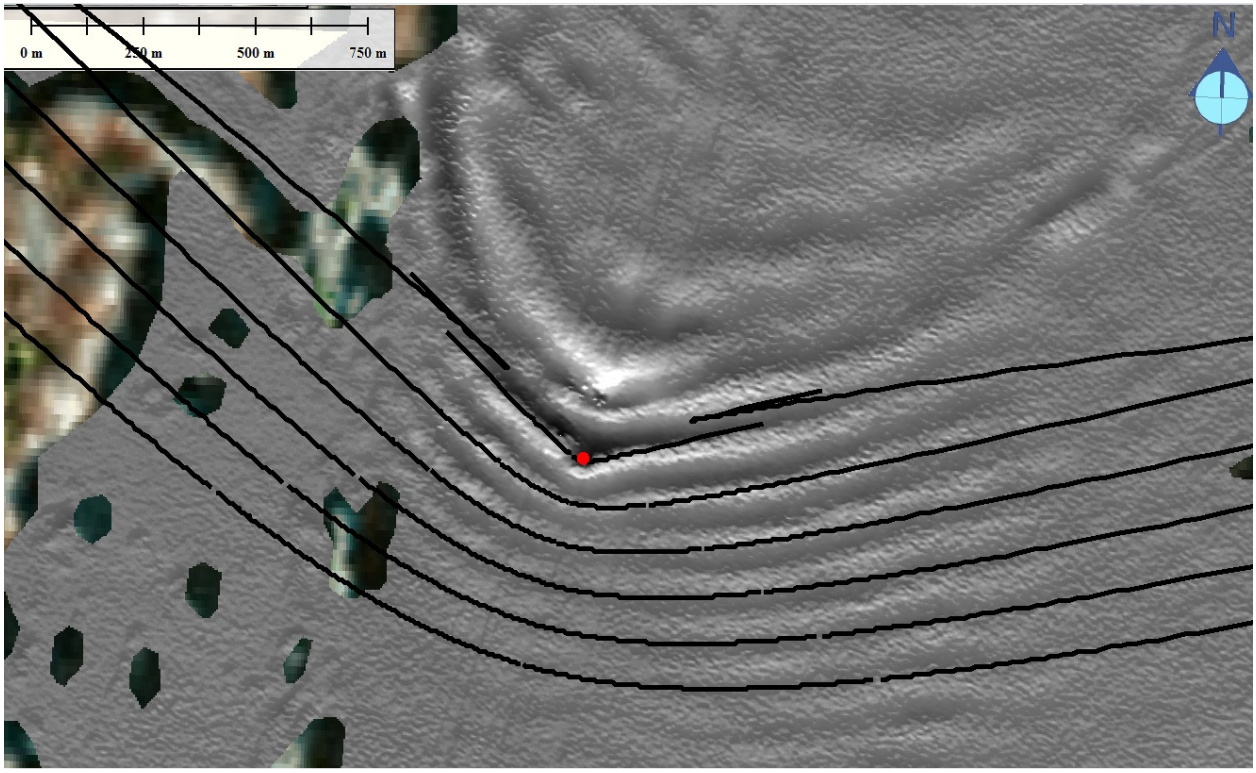

Figure 9. The comparison of the theoretical wave patterns (black lines) with the satellite-derived wave patterns (Source TanDEM-X, © DLR 2015). Red circle is the probable location of the truck in the satellite-derived data.

Theoretical wave patterns shown in Figure 9 are generally similar to their satellite-derived counterparts both with respect the shape of the waves and wavelengths. The theoretical wavelength and deflection of the road in front of the truck will be compared with satellite-based results later in the paper. Note that the satellite-derived data belong to a 10-seconds long period while the theoretical wave pattern is a snapshot. The authors expect that the satellite-derived and theoretical wave patterns converge for regions far from the truck.

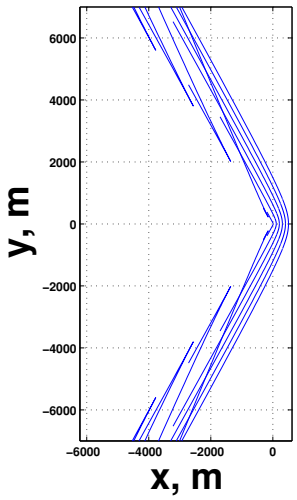

Figure 10. Theoretical wave patterns for $E = 5\ GPa$ and $h = 1.07\ m$ while other properties and conditions are given in Table 1. Note that the southbound truck is at $(0, 0)$. Waves are not seen over a region behind the truck.

Figure 11 compares the vertical displacement of the road in front of the truck, for properties and conditions for the southbound case given in Table 1, with the satellite-derived displacement. Since the theoretical deflections are based on an asymptotic solution, the deflections calculated are probably incorrect close to the moving source. Applicability of Equation (5) is suggested to be limited to distances more than one to two wavelengths away from the moving load. For the present paper, we calculate the vertical deflection of the road in front of the truck for distances associated with the phase value of $K = \frac{9\pi}{4} rad$ or larger. The theoretical deflection of the road behind the truck is theoretically zero (see shadow zone in Figure 9 and Figure 10). To calculate the theoretical deflections shown in Figure 11, the distribution of the truck weight is modelled similar to the northbound case (the truck weight is distributed over seven locations) except that the truck weight is assumed to be on the central plane shown in Figure 4b.

It is known that the effective Young's modulus of ice depends on the rate at which the ice is loaded (Sinha, 1979; Gold and Sinha, 1980); the higher the loading frequency is, the higher the effective modulus is. For the case when the wavelength is 100 m when the speed is 16 m/s, the loading rate is 0.16 Hz. At this loading rate the effective Young's modulus is approximately 7.6 GPa, for the ice grain size of 3~10 mm. Figure 11 shows the 10-seconds deflections for this higher value of the effective Young's modulus as well as the smaller value of 5 GPa for two different ice thickness values. An increase in either the effective Young's modulus or ice thickness decreases the deflections and increases the wavelength, Figure 11. Among the four modelled combinations of ice thickness and effective Young's modulus, the curve associated with the smallest thickness and modulus overestimates the deflections and underestimates the wavelength. For the other extreme case of the larger ice thickness and modulus, the deflections are underestimated and wavelength is overestimated.

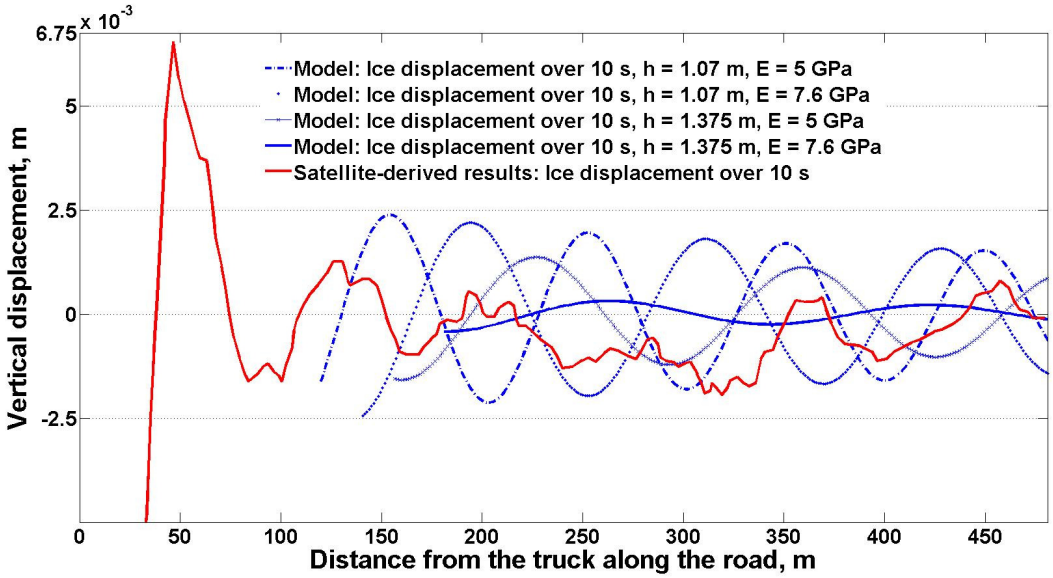

Figure 11. The theoretical and satellite-derived displacements of the ice road surface for the southbound case. Two different ice road thicknesses and effective Young's moduli are considered. Satellite data source TanDEM-X, © DLR 2015.

Conclusions and Recommendations for Future Work

The response of the TCWR ice road over Gordon Lake to moving loads was theoretically modelled in the present paper. Ice is modelled as a linearly elastic plate interacting with an underneath inviscid, incompressible fluid. The theoretical 10-seconds vertical displacement of the road was compared with satellite-derived results for two separate cases: 1) a heavy slow truck and 2) a light fast truck. Theory predicts that when the speed of the moving load is higher than a value, named the critical speed, there will be steady waves in the ice road. This prediction was verified by remotely-sensed vertical ice displacements data. Theory also predicts that when the moving load is fast enough, there is a shadow zone behind the load where the ice road is not deflected. Satellite-derived ice displacement data supports this prediction. For the purpose of the present study, a certain number of assumptions were made, leading to uncertainties. Despite these uncertainties and uncertainties in satellite-derived product, theoretical displacements and wave patterns appear to agree well with satellite-derived data.

What these analyses seem to indicate is that the speed of southbound vehicles on the TCWR is currently exceeding the critical speed as defined earlier in this paper. They also suggest that load-induced stresses vanish about 100 m away from the vehicle, which, in turn, would indicate the 500 m minimum spacing between vehicles could be reassessed if it is governed by ice strength considerations.

Future efforts to further confirm these results could focus on (1) lowering uncertainties in contributing factors including truck speed, truck weight, ice thickness and lake depth, (2) direct numerical solution of the governing equations to lift the limitation of the presently employed asymptotic method and to enable the prediction of deflections close to the fast moving load, (3) considering the full viscoelastic response, instead of the elastic contribution only, of the ice road to possibly lower the difference between the theoretically predicted displacements and wavelengths for the case of the light fast truck.

Acknowledgements

The first author thanks Fausto Milinazzo for help in understanding details of theoretical wave modelling, Duncan Cooke for providing Gordon Lake bathymetry data, Robert Frederking for sharing his knowledge about the topic of bearing capacity of ice. The German Aerospace Centre (DLR) is acknowledged for the provision of TanDEM-X data and the Arctic Program of the National Research Council of Canada for financially supporting the work of the first and fourth authors. The second and third authors received financial support from the Climate Change Geoscience Program and the Polar Continental Shelf Program of Natural Resources Canada. The Tibbitt-to-Contwoyto Winter Road (TCWR) Joint Venture Ltd. is acknowledged for logistical support and information on ice road management practices.

References

Anonymous, 2015. "Tibbitt to Contwoyto Winter Road Joint Venture. Winter Road Regulations and Rules of the Road". Guidelines issued by Diavik Diamond Mines Inc., BHP Billiton Diamonds Inc., and DeBeers Canada Inc.

Beltaos, S., 1981. "Field Studies on the Response of Floating Ice Sheets to Moving Loads". *Canadian Journal of Civil Engineering*, 8, p. 1-8.

Davys, J., Hosking, R. and Sneyd, A., 1985. "Waves due to a Steadily Moving Source on a Floating Ice Plate". *Journal of Fluid Mechanics*, 158, p. 269-287.

Gold, L.W., and Sinha, N.K., 1980. "The Rheological Behaviour of Ice at Small Strains". In Physics and Mechanics of Ice; PerTryde, Ed.; Springer-Verlag: Berlin, p. 117-128.

Hayley, D. and Proskin, S., 2008. "Managing the Safety of Ice Covers Used for Transportation in an Environment of Climate Warming". Proceedings of the 4th Canadian Conference on Geohazards, May 2008, Quebec, Canada.

Kheysin, R.K., 1963. "Moving Loads on an Elastic Plate, Floating on the Surface of an Ideal Liquid". *Mechanika i Mashinostroenie*, 1, p. 178-180.

Krieger, G., Zink, M., Bachmann, M., Bräutigam, B., Schulze, D., Martone, M., Rizzoli, P., Steinbrecher, U., Walter Antony, J., De Zan, F., Hajnsek, I., Papathanassiou, K., Kugler, F., Rodriguez Cassola, M., Younis, M., Baumgartner, S., López-Dekker, P., Prats, P., Moreira, A., 2013. "TanDEM-X: A Radar Interferometer with Two Formation-flying Satellites". *Acta Astronautica*, 89, p. 83-98.

Lighthill, M., 1978. "Waves in Fluids". Cambridge University Press, Cambridge [England].

Masterson, D.M., 2009. "State of the Art of Ice Bearing Capacity and Ice Construction". *Cold Regions Science and Technology*, 58, p. 99-112.

Milinazzo, F., Shinbrot, M. and Evans, N., 1995. "A Mathematical Analysis of the Steady Response of Floating Ice to the Uniform Motion of a Rectangular Load". *Journal of Fluid Mechanics*, 287, p. 173-197.

Moore, J.W., 1981. "Benthic Algae in Littoral and Profundal Areas of a Deep Subarctic Lake". *Canadian Journal of Botany*, 59, p. 1026-1033.

Nevel, D.E. 1970. "Moving Loads on a Floating Ice Sheet". US Army CRREL Res. Rep. 261.

Sinha, N. K., 1978. “Short-term Rheology of Polycrystalline Ice”. *Journal of Glaciology*, 21, p. 457-473.

Sinha, N.K., and Cai, B., 1996. “Elasto-delayed-elastic Simulation of Short-term Deflection of Fresh-water Ice Covers”. Cold Regions Science and Technology, 24, p. 221-235.

Squire, V., Hosking, R., Kerr, A. and Langhorne, P. 1996. “Moving Loads on Ice Plates”. Springer, Netherlands.

Sunberg-Falkenmark, M., 1963. “Resultat av belastningsforsok pa is, utforda av Samarbetsgruppen for isbarighetsforsok 1959-1961” (in Swedish). Notiser Och Preliminara Rapporter, Serie Hydrologi 1, Sveriges Meteorologiska och Hydrologiska Institute, Stockholm, Sweden.

Takizawa, T., 1988. “Response of a Floating Sea Ice Sheet to a Steadily Moving Load”. *Journal of Geophysical Research*, 93, p. 5100-5112.

Timco, G.W. and O'Brien, S., 1994. “Flexural Strength Equation for Sea Ice”. *Cold Regions Science and Technology*, 22, p. 285-298.

Timoshenko, S. and Woinowsky-Krieger, S., 1959. “Theory of Plates and Shells”. McGraw-Hill, New York.

Van der Sanden, J.J. and N.H. Short, 2016. “Radar Satellites Measure Ice Cover Displacements Induced by Moving Vehicles”. Submitted to *Cold Regions Science and Technology*.

Wilson, J.T., 1955. “Coupling Between Moving Loads and Flexural Waves in Floating Ice Sheets”. US Army CRREL Res. Rep. 34.

Wilson, J.T., 1958. “Moving Loads on Floating Ice Sheets”. University of Michigan Research Institute Report, Project 2432, Michigan, USA.